Available online at www.sciencedirect.com
ScienceDirect
Journal of Computational Physics 223 (2007) 89–107
JOURNAL OF COMPUTATIONAL PHYSICS
www.elsevier.com/locate/jcp

Solving transient conduction and radiation heat transfer problems using the lattice Boltzmann method and the finite volume method

Subhash C. Mishra *, Hillol K. Roy

Department of Mechanical Engineering, Indian Institute of Technology Guwahati, Guwahati 781039, India

Received 23 July 2005; received in revised form 16 March 2006; accepted 30 August 2006
Available online 17 October 2006

Abstract

The lattice Boltzmann method (LBM) was used to solve the energy equation of a transient conduction–radiation heat transfer problem. The finite volume method (FVM) was used to compute the radiative information. To study the compatibility of the LBM for the energy equation and the FVM for the radiative transfer equation, transient conduction and radiation heat transfer problems in 1-D planar and 2-D rectangular geometries were considered. In order to establish the suitability of the LBM, the energy equations of the two problems were also solved using the FVM of the computational fluid dynamics. The FVM used in the radiative heat transfer was employed to compute the radiative information required for the solution of the energy equation using the LBM or the FVM (of the CFD). To study the compatibility and suitability of the LBM for the solution of energy equation and the FVM for the radiative information, results were analyzed for the effects of various parameters such as the scattering albedo, the conduction–radiation parameter and the boundary emissivity. The results of the LBM–FVM combination were found to be in excellent agreement with the FVM–FVM combination. The number of iterations and CPU times in both the combinations were found comparable.

Keywords: Lattice Boltzmann method; Finite volume method; Participating medium; Radiative heat transfer; Conduction–radiation

1. Introduction

In the recent years, usage of the lattice Boltzmann method (LBM) as an alternative approach to the conventional computational fluid dynamics (CFD) solvers such as the finite element method (FEM), the finite difference method (FDM) and the finite volume method (FVM) has gained momentum [1–9]. As a different approach from the CFD solvers, the LBM uses simple microscopic kinetic models to simulate complex transport phenomena. In comparison to the CFD solvers, the advantages of the LBM include among other simple calculation procedure, simple and efficient implementation for parallel computation, easy and robust

* Corresponding author. Tel.: +91 361 2582660; fax: +91 361 2690762.
E-mail address: scm_iitg@yahoo.com (S.C. Mishra).

0021-9991/$ - see front matter © 2006 Elsevier Inc. All rights reserved.
doi:10.1016/j.jcp.2006.08.021

Nomenclature

A	area
a	anisotropy factor
b	number of discrete directions in the lattice
c_p	specific heat
$\vec{e}_i$	propagation velocity in the direction i in the lattice
f_i	particle distribution function in the i direction
$f_i^{(0)}$	equilibrium particle distribution function in the i direction
G	incident radiation
I	intensity
k	thermal conductivity
M_θ	number of discrete θ directions
M_ϕ	number of discrete ϕ directions
m	index for direction
N	conduction–radiation parameter, $\kappa\beta/(4\sigma T_{\text{ref}}^3)$
$\hat{n}$	outer normal
P	cell center
$\vec{q}_{\text{R}}$	radiative heat flux
$\vec{r}$	position, $r(x, y, z)$
S	source term
T	temperature
t	time
V	volume of the cell
w	weight in the LBM
X, Y, Z	length of the rectangular enclosure in x, y and z directions

Greek symbols

α	thermal diffusivity
β	extinction coefficient
γ	finite difference weighing factor
ε	emissivity
θ	polar angle
κ_{a}	absorption coefficient
ξ	non-dimensional time, $\alpha\beta^2 t$
ρ	density
σ	Stefan–Boltzmann constant ($=5.670\times10^{-8}$ W/m^2 K^4)
σ_{s}	scattering coefficient
τ	relaxation time
Φ	scattering phase function
ϕ	azimuthal angle
ω	scattering albedo
Ω	direction in the FVM and rate of change of the particle distribution function f_i in the LBM
$\Delta\Omega$	elemental solid angle

Subscripts

E,W, N, S, F, B	east, west, north, south, front and back
b	boundary
x, y, z	x, y and z reference faces
e	exit
i	inlet

k, l	index of discrete polar and azimuthal angles, respectively
P	value at the cell center
Superscript	
m	index for direction

handling of complex geometries and high computational performance with regard to stability and accuracy [1–9].

The LBM has found extensive usage in the fluid mechanics [3,5–8] and its recent application to problems involving conductive, convective and/or radiative heat transfer has been very encouraging [10–14]. Shan [10] and Mezrhab et al. [11] used the LBM to analyze the convective flows. Ho et al. [12,13] solved a non-Fourier heat conduction problem in a planar medium using the LBM. Solidification of a planar medium using the LBM was analyzed by Jiaung et al. [14]. Chatterjee and Chakraborty [15] used the LBM to analyze solid–liquid phase transitions in the presence of thermal diffusion. Mishra and Lankadasu [16] applied the LBM to solve the energy equation of transient conduction and radiation heat transfer in a planar medium with or without heat generation. They used the discrete transfer method (DTM) [17] to compute the radiative information. Mishra et al. [18] used the LBM to solve the energy equation of a transient conduction–radiation heat transfer in a 2-D square enclosure. In their study, they used the collapsed dimension method (CDM) [19] to compute the radiative information. Application of the LBM to analyze the solidification of a semitransparent planar layer was extended by Raj et al. [20]. They used the DTM [17] to compute the radiative information. Gupta et al. [21] used the concept of a variable relaxation time in the LBM and then solved the energy equation of a temperature dependent transient conduction and radiation heat transfer in a planar medium. They used the discrete ordinate method (DOM) [22] for the determination of the radiative information. In all the previous applications to the conduction–radiation heat transfer problems, the LBM was found to provide accurate results and compatibilities of the LBM for solution of energy equation and the DTM, the CDM and the DOM for the determination of radiative information were established. The DTM in [18,20] and the DOM in [21] with the LBM were applied to 1-D planar geometry.

In radiative heat transfer, the finite volume method (FVM) [23,24] is extensively used to compute the radiative information. This method is a variant of the DOM [22]. However, unlike the DOM, it does not suffer from the false-scattering [24]. In this method, the ray-effect is also less pronounced [24]. Since the FVM for the radiative heat transfer utilizes the same concept as that of the FVM of the CFD, in conjugate mode problems, its computational grids are compatible with the FVM grids that are utilized in the solution of the momentum and energy equations [25,26]. Thus, although the FVM for the radiative heat transfer is only a 15-year old method, it enjoys more popularity than the DTM, and the DOM.

In solving the energy equations of the combined radiation, conduction and/or convection heat transfer problems using the conventional CFD based methods such as the FDM and the FVM, robustness of the FVM in providing radiative information is well established [23,24]. Since the LBM is relatively a new method and for the solution of combined radiation, conduction and/or convection mode problems its application is very recent, the FVM has so far not been used in conjunction with the LBM to solve any such problems. The present article is thus aimed at extending the application of both the LBM and the FVM to a relatively new class of problems.

The objective of the present work is to establish the compatibility of the LBM for the solution of the energy equation and the FVM for the determination of radiative information. One other objective is also to see how the LBM–FVM combination performs against the FVM–FVM combination in which the energy equation is solved using the FVM of the CFD and the radiative information is computed using the FVM of radiative heat transfer. Towards this goal, transient conduction and radiation heat transfer problems in 1-D planar and 2-D rectangular enclosures are considered. For various parameters like the scattering albedo, the conduction–radiation parameter and the boundary emissivity, results of the LBM–FVM and the FVM–FVM are compared with those reported in the literature and compared against each other. Effects of the spatial and angular res-

olutions on the results are also made. The number of iterations and CPU times for the converged solutions are also reported.

The paper is organized as follows. In Section 2, the formulation of the FVM to calculate radiative information required for the energy equation is provided first. The methodology of the LBM is discussed next. Implementation of the boundary conditions is briefly discussed after that. The solution procedure has been discussed in Section 3. The results of the parametric study and the comparison are presented in Section 4. Conclusions and recommendations are made at the end.

2. Formulation

In the absence of convection and heat generation, for a homogeneous medium, the energy equation is given by

$$\rho c_p \frac{\partial T}{\partial t} = k\nabla^2 T - \nabla \cdot \vec{q}_R \tag{1}$$

where ρ is the density, c_p is the specific heat, k is the thermal conductivity and $\vec{q}_R$ is the radiative heat flux. With radiative information $\nabla \cdot \vec{q}_R$ computed using any of the methods such as the DTM [17], the CDM [19], the DOM [22] and the FVM [23,24], Eq. (1) can be solved using any of the conventional CFD methods such as the FDM, FEM and the FVM or an alternative approach, the LBM.

The FVM in the radiative heat transfer being the latest and the most versatile method for the computation of radiative information $\nabla \cdot \vec{q}_R$ and the LBM being seen as a potential substitute of the CFD based methods such as the FDM, the FEM and the FVM, in the following pages we briefly discuss the methodology of the FVM for the computation of $\nabla \cdot \vec{q}_R$ and the procedure in the LBM to solve the energy equation (Eq. (1)). The coupling of the methods of two different kinds is also discussed.

2.1. The finite volume method (FVM)

The radiative transfer equation (RTE) in any direction $\hat{s}$ identified by the solid angle Ω about an elemental solid angle $d\Omega$ is given by [27]

$$\frac{dI(\vec{r},\Omega)}{ds} = -(\kappa_a + \sigma_s)I(\vec{r},\Omega) + \kappa_a\left(\frac{\sigma T^4(\vec{r})}{\pi}\right) + \frac{\sigma_s}{4\pi}\int_{\Omega'=4\pi} I(\vec{r},\Omega')\Phi(\Omega,\Omega')d\Omega' \tag{2}$$

where κ_a is the absorption coefficient, σ_s is the scattering coefficient and Φ is the scattering phase function. Eq. (2) can be written as

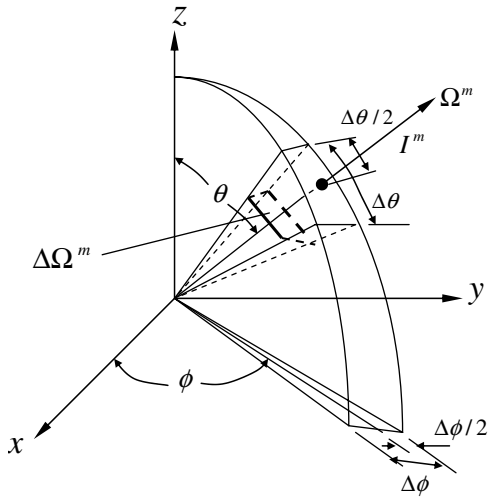

Fig. 1. Intensity I^m in direction Ω^m in the center of the elemental sub-solid angle $\Delta\Omega^m$.

$$\frac{\mathrm{d}I}{\mathrm{d}s} = -\beta I + S \tag{3}$$

where $\beta = \kappa_a + \sigma_s$ is the extinction coefficient and S is the source term given by

$$S = \kappa_a\left(\frac{\sigma T^4}{\pi}\right) + \frac{\sigma_s}{4\pi}\int_{\Omega'=4\pi} I(\Omega')\Phi(\Omega,\Omega')\mathrm{d}\Omega' \tag{4}$$

Resolving Eq. (1) along the Cartesian coordinate directions (Fig. 1) and integrating it over the elemental solid angle $\Delta\Omega^m$, we get

$$\frac{\partial I^m}{\partial x}D_x^m + \frac{\partial I^m}{\partial y}D_y^m + \frac{\partial I^m}{\partial z}D_z^m = -\beta I^m \Delta\Omega^m + S^m\Delta\Omega^m \tag{5}$$

If $\hat{n}$ is the outward normal to a surface, then D^m is given by

$$D^m = \int_{\Delta\Omega^m}(\hat{n}\cdot\hat{s}^m)\mathrm{d}\Omega \tag{6}$$

where the direction $\hat{s}^m = (\sin\theta^m\cos\phi^m)\hat{i} + (\sin\theta^m\sin\phi^m)\hat{j} + (\cos\theta^m)\hat{k}$. When $\hat{n}$ is pointing towards one of the positive coordinate directions, D_x^m, D_y^m and D_z^m are given by

$$D_x^m = \int_{\Delta\Omega^m}\sin\theta\cos\phi\,\mathrm{d}\Omega = \int_{\phi^m-\frac{\Delta\phi^m}{2}}^{\phi^m+\frac{\Delta\phi^m}{2}}\int_{\theta^m-\frac{\Delta\theta^m}{2}}^{\theta^m+\frac{\Delta\theta^m}{2}}\cos\phi\sin^2\theta\,\mathrm{d}\theta\,\mathrm{d}\phi$$
$$= \cos\phi^m\sin\left(\frac{\Delta\phi^m}{2}\right)[\Delta\theta^m - \cos 2\theta^m\sin(\Delta\theta^m)] \tag{7a}$$

$$D_y^m = \int_{\Delta\Omega^m}\sin\theta\sin\phi\,\mathrm{d}\Omega = \int_{\phi^m-\frac{\Delta\phi^m}{2}}^{\phi^m+\frac{\Delta\phi^m}{2}}\int_{\theta^m-\frac{\Delta\theta^m}{2}}^{\theta^m+\frac{\Delta\theta^m}{2}}\sin\phi\sin^2\theta\,\mathrm{d}\theta\,\mathrm{d}\phi$$
$$= \sin\phi^m\sin\left(\frac{\Delta\phi^m}{2}\right)[\Delta\theta^m - \cos 2\theta^m\sin(\Delta\theta^m)] \tag{7b}$$

$$D_z^m = \int_{\Delta\Omega^m}\cos\theta\,\mathrm{d}\Omega = \int_{\phi^m-\frac{\Delta\phi^m}{2}}^{\phi^m+\frac{\Delta\phi^m}{2}}\int_{\theta^m-\frac{\Delta\theta^m}{2}}^{\theta^m+\frac{\Delta\theta^m}{2}}\cos\theta\sin\theta\,\mathrm{d}\theta\,\mathrm{d}\phi = \sin\theta^m\cos\theta^m\sin(\Delta\theta^m)\Delta\phi^m \tag{7c}$$

For $\hat{n}$ pointing towards the negative coordinate directions, signs of D_x^m, D_y^m and D_z^m are opposite to what are obtained from Eq. (7). In Eq. (5), $\Delta\Omega^m$ is given by

$$\Delta\Omega^m = \int_{\Delta\Omega^m}\mathrm{d}\Omega = \int_{\phi^m-\frac{\Delta\phi^m}{2}}^{\phi^m+\frac{\Delta\phi^m}{2}}\int_{\theta^m-\frac{\Delta\theta^m}{2}}^{\theta^m+\frac{\Delta\theta^m}{2}}\sin\theta\,\mathrm{d}\theta\,\mathrm{d}\phi = 2\sin\theta^m\sin\left(\frac{\Delta\theta^m}{2}\right)\Delta\phi^m \tag{8}$$

For the limits of integrations in Eqs. (7) and (8), please refer to Fig. 1.

Integrating Eq. (8) over the control volume and using the concept of the FVM for the CFD, we get

$$[I_E^m - I_W^m]A_{EW}D_x^m + [I_N^m - I_S^m]A_{NS}D_y^m + [I_F^m - I_B^m]A_{FB}D_z^m = [-\beta V I_P^m + V S_P^m]\Delta\Omega^m \tag{9}$$

where A_{EW}, A_{NS} and A_{FB} are the areas of the x-, y- and z-faces of the 3-D control volume, respectively. In Eq. (9), I with suffixes E, W, N, S, F and B designate east, west, north, south, front and back control surface average intensities, respectively. On the right-hand-side of Eq. (9), $V = \mathrm{d}x\times\mathrm{d}y\times\mathrm{d}z$ is the volume of the cell and I_P^m and S_P^m are the intensities and source terms at the cell center P, respectively.

In any discrete direction Ω^m, if a linear relationship among the two cell-surface intensities and cell-center intensity I_P^m is assumed, then

$$I_P^m = \gamma_x I_E^m + (1-\gamma_x)I_W^m = \gamma_y I_N^m + (1-\gamma_y)I_S^m = \gamma_z I_F^m + (1-\gamma_z)I_B^m \tag{10}$$

where γ is the finite difference weighting factor and its value is normally considered to be 0.5. While marching from the first octant of a 3-D enclosure (Fig. 4a) for which D_x^m, D_y^m and D_z^m are all positive, I_P^m in terms of known cell-surface intensities can be written as

$$I_{\mathrm{P}}^{m}=\frac{\frac{D_x^m A_{\mathrm{EW}}}{\gamma_x} I_{\mathrm{W}}^{m}+\frac{D_y^m A_{\mathrm{NS}}}{\gamma_y} I_{\mathrm{S}}^{m}+\frac{D_z^m A_{\mathrm{FB}}}{\gamma_z} I_{\mathrm{B}}^{m}+(V\Delta\Omega^m)S_{\mathrm{P}}^{m}}{\frac{D_x^m A_{\mathrm{E}}}{\gamma_x}+\frac{D_y^m A_{\mathrm{N}}}{\gamma_y}+\frac{D_y^m A_{\mathrm{F}}}{\gamma_z}+\beta V\Delta\Omega^m} \tag{11}$$

where

$$A_{\mathrm{EW}}=(1-\gamma_x)A_{\mathrm{E}}+\gamma_x A_{\mathrm{W}}, A_{\mathrm{NS}}=(1-\gamma_y)A_{\mathrm{N}}+\gamma_y A_{\mathrm{S}}, A_{\mathrm{FB}}=(1-\gamma_z)A_{\mathrm{F}}+\gamma_z A_{\mathrm{B}} \tag{12}$$

are the averaged areas. When any one of the D_x^m, D_y^m or D_z^m is negative, marching starts from other corners (Fig. 4a). In this case, a general expression of I_{P}^m in terms of known intensities and source term can be written as

$$I_{\mathrm{P}}^{m}=\frac{\frac{|D_x^m|A_x}{\gamma_x} I_{x_i}^{m}+\frac{|D_y^m|A_y}{\gamma_y} I_{y_i}^{m}+\frac{|D_z^m|A_z}{\gamma_z} I_{z_i}^{m}+(V\Delta\Omega^m)S_{\mathrm{P}}^{m}}{\frac{|D_x^m|A_{x_e}}{\gamma_x}+\frac{|D_y^m|A_{y_e}}{\gamma_y}+\frac{|D_z^m|A_{z_e}}{\gamma_z}+\beta V\Delta\Omega^m} \tag{13}$$

where in Eq. (13), x_i, y_i and z_i suffixes over I^m are for the intensities entering the control volume through x-, y- and z-faces, respectively and A_x, A_y and A_z are given by

$$A_x=(1-\gamma_x)A_{x_e}+\gamma_x A_{x_i}, \quad A_y=(1-\gamma_y)A_{y_e}+\gamma_y A_{y_i}, \quad A_{\mathrm{FB}}=(1-\gamma_z)A_{z_e}+\gamma_z A_{z_i} \tag{14}$$

In Eq. (13) A with suffixes x_i, y_i and z_i represent control surface areas through which intensities enter the control volume, while A with suffixes x_e, y_e and z_e represent control surface areas through which intensities leave the control volume.

For a linear anisotropic phase function $\Phi(\Omega,\Omega')=1+a\cos\theta\cos\theta'$, the source term S at any location $\vec{r}$ is given by

$$S=\kappa_{\mathrm{a}}\left(\frac{\sigma T^4}{\pi}\right)+\left(\frac{\sigma_{\mathrm{s}}}{4\pi}\right)\int_0^{2\pi}\int_0^{\pi} I(\theta',\phi')(1+a\cos\theta\cos\theta')\sin\theta'\,\mathrm{d}\theta'\,\mathrm{d}\phi' \tag{15}$$

which in terms of the incident radiation G and net radiative heat flux q_{R} is written as

$$S=\kappa_{\mathrm{a}}\left(\frac{\sigma T^4}{\pi}\right)+\frac{\sigma_{\mathrm{s}}}{4\pi}[G+a\cos\theta q_{\mathrm{R}}] \tag{16}$$

In Eq. (16), G and q_{R} are given by and numerically computed from the following

$$G=\int_{\Omega=0}^{4\pi} I(\Omega)\mathrm{d}\Omega=\int_{\phi=0}^{2\pi}\int_{\theta=0}^{\pi} I(\theta,\phi)\sin\theta\,\mathrm{d}\theta\,\mathrm{d}\phi\approx\sum_{k=1}^{M_\phi}\sum_{l=1}^{M_\theta} I^m(\theta_l^m,\phi_k^m)2\sin\theta_l^m\sin\left(\frac{\Delta\theta_l^m}{2}\right)\Delta\phi_k^m \tag{17}$$

where M_θ and M_ϕ are the number of discrete points considered over the complete span of the polar angle ($0\leqslant\theta\leqslant\pi$) and azimuthal angle ($0\leqslant\phi\leqslant 2\pi$), respectively. Therefore, $M_\theta\times M_\phi$ constitute the number of discrete directions in which intensities are considered at any point.

$$\begin{aligned} q_{\mathrm{R}} &= \int_{\Omega=0}^{4\pi} I(\Omega)\cos\theta\,\mathrm{d}\Omega=\int_{\phi=0}^{2\pi}\int_{\theta=0}^{\pi} I(\theta,\phi)\cos\theta\sin\theta\,\mathrm{d}\theta\,\mathrm{d}\phi \\ &\approx \sum_{k=1}^{M_\phi}\sum_{l=1}^{M_\theta} I^m(\theta_l^m,\phi_k^m)\sin\theta_l^m\cos\theta_l^m\sin(\Delta\theta_l^m)\Delta\phi_k^m \end{aligned} \tag{18}$$

While marching from any of the corners, evaluation of Eq. (13) requires knowledge of the boundary intensity. For a diffuse-gray boundary/wall having temperature T_{b} and emissivity ε_{b}, the boundary intensity I_{b} is computed from

$$I_{\mathrm{b}}=\frac{\varepsilon_{\mathrm{b}}\sigma T_{\mathrm{b}}^4}{\pi}+\left(\frac{1-\varepsilon_b}{\pi}\right)\sum_{k=1}^{M_\phi}\sum_{l=1}^{M_\theta/2} I^m(\theta_l^m,\phi_k^m)\sin\theta_l^m\cos\theta_l^m\sin\Delta\theta_l^m\Delta\phi_k^m \tag{19}$$

In Eq. (19), the first and the second terms represent the emitted and the reflected components of the boundary intensity, respectively.

Once the intensity distributions are known, radiative information $\nabla\cdot\vec{q}_{\mathrm{R}}$ required for the energy equation is computed from

$$\nabla \cdot \vec{q}_{\mathrm{R}} = \beta(1-\omega)\left(4\pi\frac{\sigma T^4}{\pi} - G\right) \tag{20}$$

where in Eq. (20), $\omega = \sigma_s/\beta$ is the scattering albedo.

2.2. Lattice Boltzmann method (LBM)

The starting point of the LBM is the kinetic equation which for a 3-D geometry is given by [3,5,7,8]

$$\frac{\partial f_i(\vec{r},t)}{\partial t} + \vec{e}_i \cdot \nabla f_i(\vec{r},t) = \Omega_i, \quad i = 1,2,3,\ldots,b \tag{21}$$

where f_i is the particle distribution function denoting the number of particles at the lattice node $\vec{r} = (\vec{r}(x,y,z))$ and time t moving in direction i with velocity $\vec{e}_i$ along the lattice link $\Delta\vec{r} = \vec{e}_i\Delta t$ connecting the nearest neighbors and b is the number of directions in a lattice through which the information propagates. The term Ω_i represents the local change in f_i due to particle collisions. Using the single time relaxation of the Bhatanagar–Gross–Krook (BGK) approximation, the discrete Boltzmann equation is given by [3,5,7,8]

$$\frac{\partial f_i(\vec{r},t)}{\partial t} + \vec{e}_i \cdot \nabla f_i(\vec{r},t) = -\frac{1}{\tau}[f_i(\vec{r},t) - f_i^{(0)}(\vec{r},t)] \tag{22}$$

where τ is the relaxation time and $f_i^{(0)}$ is the equilibrium distribution function. In the LBM, lattices depend upon the geometries. D1Q2 and D1Q3 are the lattices used in 1-D geometries, while D2Q7 and D2Q9 are the lattices used in 2-D geometries. In 3-D geometries, normally D3Q15 and D3Q19 lattices are used. In all these lattices, the number following D denotes the dimension and the number following Q denotes the number of directions through which the particle distribution function f_i propagates to the nearest neighbors. In the lattice having odd number of directions, one particle distribution function remains at rest at the lattice center.

For a given application, relaxation time τ is different for different lattices. In heat transfer problems, the relaxation time τ for the D1Q2 lattice (Fig. 2) is computed from [7,8]

$$\tau = \frac{\alpha}{|\vec{e}_i|^2} + \frac{\Delta t}{2} \tag{23}$$

For the D1Q2 lattice (Fig. 2) the two velocities $\vec{e}_i$ and their corresponding weights w_i are calculated from

$$e_1 = C, \quad e_2 = -C \tag{24}$$

$$w_1 = w_2 = \frac{1}{2} \tag{25}$$

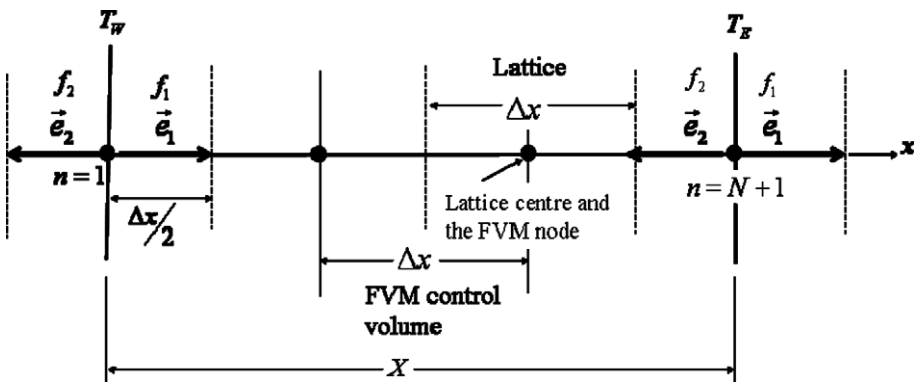

Fig. 2. D1Q2 lattice of the LBM and control volume of the FVM used in 1-D planar geometry.

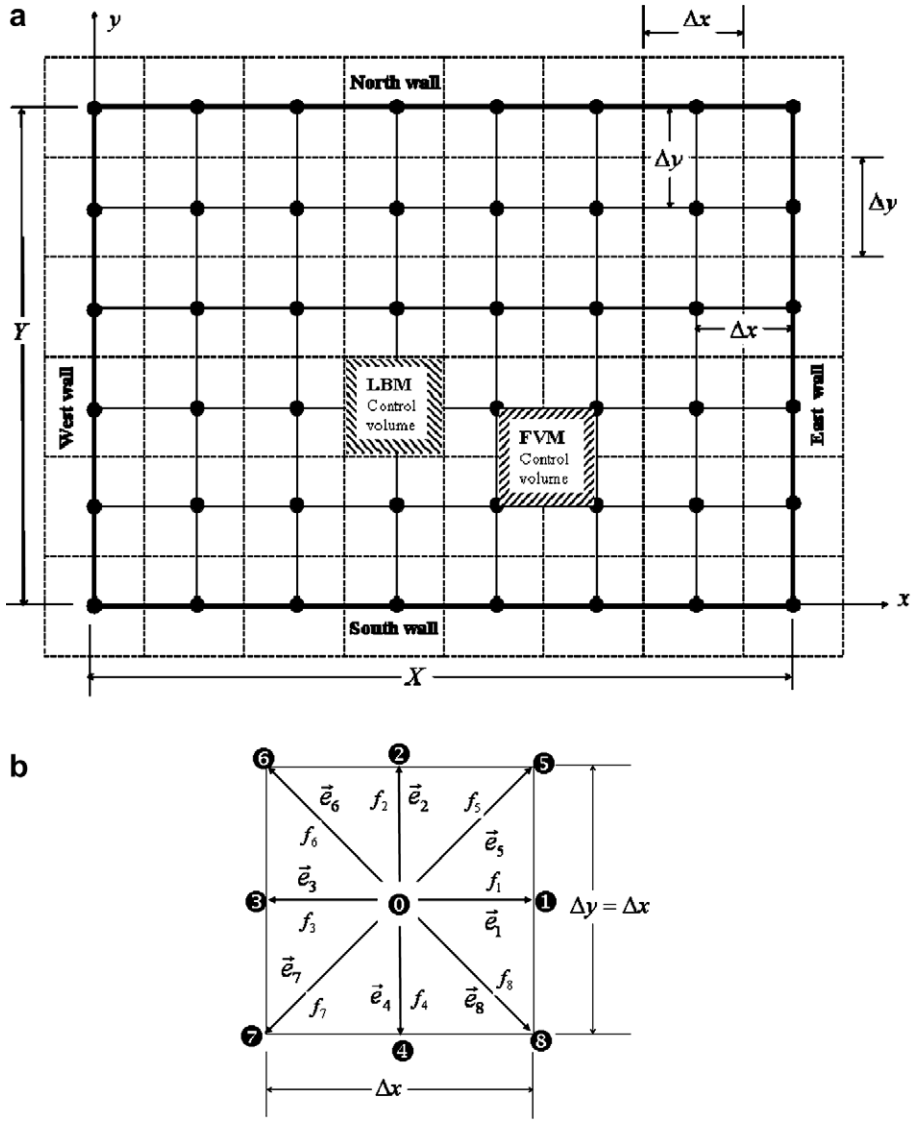

Fig. 3. (a) Arrangement of lattices and control volumes in a 2-D rectangular geometry and (b) D2Q9 lattice used in a 2-D geometry.

The relaxation time τ for the D2Q9 (Fig. 3b) and the D3Q15 (Fig. 4b) lattices is given by [7,8]

$$\tau = \frac{3\alpha}{|\vec{e}_i|^2} + \frac{\Delta t}{2} \tag{26}$$

The nine velocities $\vec{e}_i$ and their corresponding weights w_i in the D2Q9 lattice are the following:

$$\begin{aligned} e_0 &= (0,0) \\ e_{1,3} &= (\pm 1, 0) \cdot C \\ e_{2,4} &= (0, \pm 1) \cdot C \\ e_{5,6,7,8} &= (\pm 1, \pm 1) \cdot C \end{aligned} \tag{27}$$

$$w_0 = \frac{4}{9}, \quad w_{1,2,3,4} = \frac{1}{9}, \quad w_{5,6,7,8} = \frac{1}{36} \tag{28}$$

For the D3Q15 lattice (Fig. 3b), the same are given by

$$\begin{aligned} e_0 &= (0,0,0) \\ e_{1,2} &= (\pm 2,0,0)\cdot C \\ e_{3,4} &= (0,\pm 2,0)\cdot C \\ e_{5,6} &= (0,0,\pm 2)\cdot C \\ e_{7,\ldots,14} &= (\pm 1,\pm 1,\pm 1)\cdot C \end{aligned} \tag{29}$$

$$w_0 = \frac{2}{9}, \quad w_{1,\ldots,6} = \frac{1}{9}, \quad w_{7,\ldots,14} = \frac{1}{72} \tag{30}$$

It is to be noted that in the above equations, $C = \Delta x/\Delta t = \Delta y/\Delta t = \Delta z/\Delta t$ and the weights satisfy the relation $\sum_{i=1}^{b} w_i = 1$.

After discretization, Eq. (21) can be written as [7,8]

$$f_i(\vec{r} + \vec{e}_i\Delta t, t + \Delta t) = f_i(\vec{r}, t) - \frac{\Delta t}{\tau}[f_i(\vec{r}, t) - f_i^{(0)}(\vec{r}, t)] \tag{31}$$

This is the LB equation with the BGK approximation that describes the evolution of the particle distribution function f_i. The algorithm for Eq. (31) can be divided into two essential parts per time step:

- The calculation of new distribution functions f_i with respect to the right-hand-side of Eq. (31), the so-called collision.
- The streaming of the distribution functions to the next neighboring nodes, usually referred to as propagation.

In case of heat transfer problems, the temperature is obtained after summing f_i over all direction [7,8], i.e,

$$T(\vec{r}, t) = \sum_{i=0}^{b} f_i(\vec{r}, t) \tag{32}$$

To process Eq. (31), an equilibrium distribution function is required. For heat conduction problems, this is given by

$$f_i^{(0)}(\vec{r}, t) = w_i T(\vec{r}, t) \tag{33}$$

From Eqs. (32) and (33), we also have

$$\sum_{i=0}^{b} f_i^{(0)}(\vec{r}, t) = \sum_{i=0}^{b} w_i T(\vec{r}, t) = T(\vec{r}, t) = \sum_{i=0}^{b} f_i(\vec{r}, t) \tag{34}$$

Eq. (31), with definitions of temperature $T(\vec{r}, t)$ and equilibrium function $f_i^{(0)}(\vec{r}, t)$ given in Eqs. (32) and (33), respectively, provide solution of a transient heat conduction problem in the LBM. To incorporate the volumetric radiation, Eq. (31) gets modified to

$$f_i(\vec{r} + \vec{e}_i\Delta t, t + \Delta t) = f_i(\vec{r}, t) - \frac{\Delta t}{\tau}[f_i(\vec{r}, t) - f_i^{(0)}(\vec{r}, t)] - \left(\frac{\Delta t}{\rho c_p}\right) w_i \nabla \cdot \vec{q}_R \tag{35}$$

Eq. (35) is the desired equation to be used in the LBM. It is to be noted that Eq. (1) can be obtained from Eq. (34) using the Chapman–Enskog multiscale expansion. Details on derivation of Eq. (1) from Eq. (35) have been given by Mishra et al. [18].

2.3. Implementation of boundary conditions in the LBM

In applications of the LBM to heat transfer problems, temperature or flux boundary condition at any boundary can be applied using the bounce-back concept in the LBM in which particle fluxes are balanced at any point on the boundary. Because of this balancing, in the implementation of the LBM, as shown in Figs. 2–4, the LBM lattices along the boundaries always extend a distance equal to half the control volume dimen-

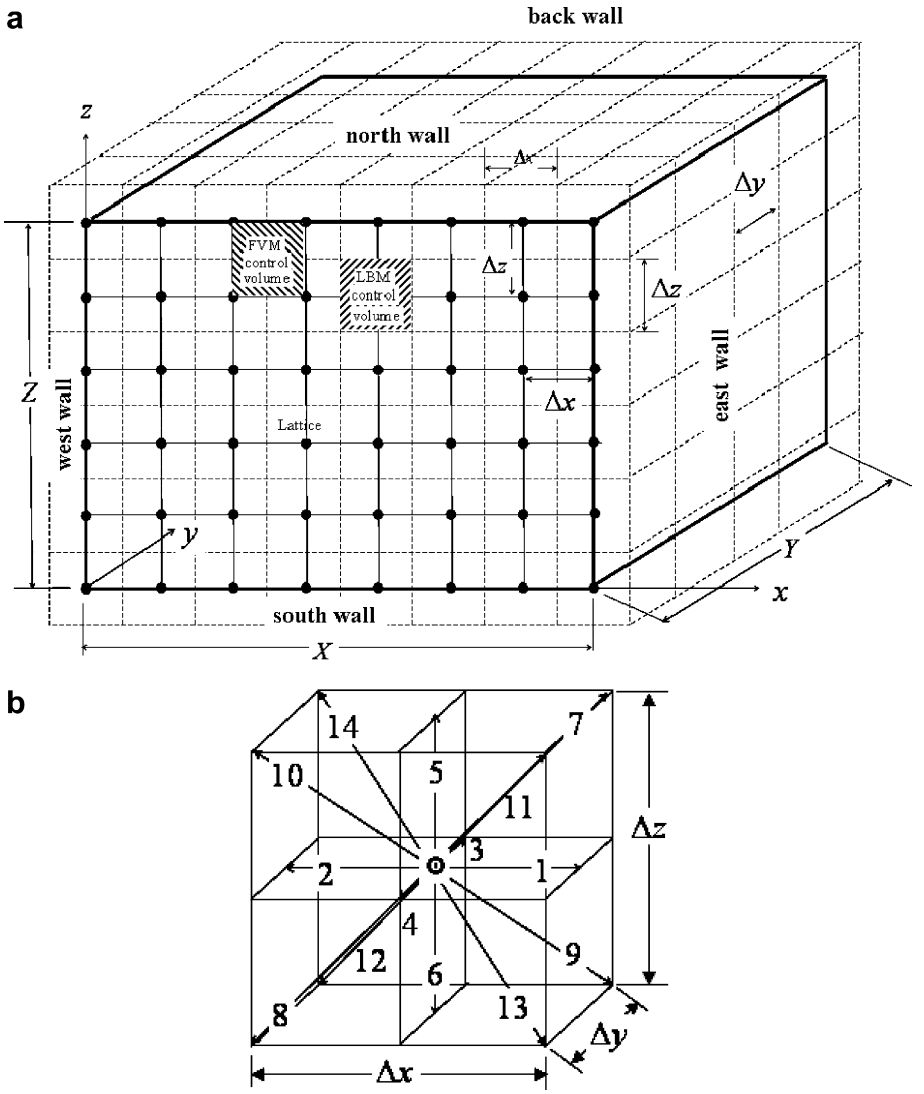

Fig. 4. (a) Arrangement of lattices and control volumes in a 3-D Cartesian geometry (b) D3Q15 lattice in a 3-D geometry.

sion in the respective coordinate directions and the lattice centers of the boundary lattices always lie along the boundaries. Details on implantation of the boundary conditions can be found in [16,18,28].

3. Solution procedure

The medium is divided into a finite number of lattices/control volumes. The control volumes of the FVM for computing the radiative information $\nabla \cdot \vec{q}_R$ and lattices in the LBM are staggered as shown in Figs. 2–4. Sizes of the lattices in the LBM and the control volumes in the FVM are taken the same.

In solving Eq. (35), $\nabla \cdot \vec{q}_R$ information is required at the lattice centers (Figs. 2–4). In the FVM for the radiative heat transfer, in any control volume, intensity distributions are computed at the mid-points of the control surfaces and at the center of the FVM control volume. Thus $\nabla \cdot \vec{q}_R$ is known only at these points (three points in 1-D, five points in 2-D and seven points in 3-D control volumes in Figs. 2–4, respectively). It is seen from Figs. 2–4 that none of these points coincide with the lattice centers. Therefore, $\nabla \cdot \vec{q}_R$ value at any lattice center is computed from the average of the $\nabla \cdot \vec{q}_R$ values of the control-surfaces surrounding that lattice center. For the lattice centers along the corners, average of the $\nabla \cdot \vec{q}_R$ values are based on $\nabla \cdot \vec{q}_R$ of the corner faces. For

any other points except the corner points along a boundary, the $\nabla \cdot \vec{q}_R$ at the lattice center is the average of $\nabla \cdot \vec{q}_R$ values of the neighboring points, that are collinear for 2-D geometries and coplanar for 3-D geometries, with the lattice center.

The procedure to solve the energy equation (Eq. (35)) is the following:

Depending upon the type of geometry, choose the lattice and accordingly compute the relaxation time τ.

1. With initial temperature field known, in the first iteration, calculate the equilibrium particle distribution function $f_i^{(0)}(\vec{r}, 0)$ from Eq. (33).
2. With initial temperature field known, calculate $\nabla \cdot \vec{q}_R$ using the FVM (Eq. (20)).
3. Calculate now the particle distribution functions $f_i(\vec{r} + \vec{e}_i \Delta t, t + \Delta t)$ using Eq. (35).
4. Propagate the particle distributions to the neighboring lattice centers.
5. Calculate the new temperature field $T(\vec{r}, t)$ using Eq. (32).
6. Check for convergence and terminate the process, if appropriate.
7. Modify the particle distribution functions locally, to satisfy the boundary conditions.
8. Compute the equilibrium particle distribution functions $f_i^{(0)}(\vec{r}, 0)$ from the new temperature field using Eq. (33) for every lattice.
9. Go to step 2.

4. Results and discussion

To validate the usage of the LBM and to show the compatibility of the FVM for the radiative information with the LBM solver for the energy equation, we consider transient conduction and radiation heat transfer in a 1-D planar and 2-D square geometries. To compare the performance of the LBM, the energy equations of the two problems were also solved using the FVM of the CFD. In both the LBM and the FVM solvers of the energy equations, radiative information $\nabla \cdot \vec{q}_R$ was computed using the FVM of the radiative heat transfer. In the FVM solver for the energy equation, we used the alternative direction implicit scheme. In the LBM–FVM (LBM for the energy equation and the FVM for the radiative information), as shown in Figs. 2 and 3, lattices in the LBM and the control volumes in the FVM for radiation were of the same size. Also in the FVM–FVM (FVM for the solution of the energy equation and FVM for the determination of radiative information) $\nabla \cdot \vec{q}_R$, the same size control volumes were used.

4.1. Conduction and radiation heat transfer in a 1-D planar medium

In this case, initially the medium is at temperature T_E. For time $t > 0$, the west boundary is maintained at T_W. The homogenous gray radiating–conducting medium is absorbing, emitting and isotropically scattering. The medium boundaries are considered diffuse-gray. Benchmark results for this problem are available in [16,29–32].

In both the FVM–FVM and the LBM–FVM, non-dimensional time step $\Delta\xi = 1.0 \times 10^{-4}(\xi = \alpha\beta^2 t)$ was considered and steady-state condition was assumed to have been achieved when the maximum variation in temperature T/T_W at any location between two consecutive time levels did not exceed 1.0×10^{-6}. In both combinations of the methods, beyond 100 control volumes/lattices and 10 directions, no significant changes in the results were observed.

It is to be noted that in case of a 1-D planar medium, radiation is azimuthally symmetric, $I(\theta, \phi) = I(\theta)$. Thus, in the FVM, only θ space was discretized into 10 directions.

In Table 1, for the two sets of boundary emissivities, the FVM–FVM and the LBM–FVM results for temperature T/T_W at three locations in the medium *viz* $x/X = 0.25$, 0.5 and 0.75 are compared at time $\xi = 0.05$ with those reported in the literature [16,29–32]. In order to compare these results, initially the entire system was considered cold $T_E = 0.0$ and for time $t > 0.0$, the west boundary was maintained at temperature T_W. The values of the parameters considered were: extinction coefficient $\beta = 1.0$, scattering albedo $\omega = 0.5$ and conduction–radiation parameter $N = \frac{\kappa\beta}{4\sigma T_W^3} = 0.1$. It is seen from the table that the FVM–FVM and the LBM–FVM results are in very good agreements with each other and they also compare very well with those reported in literatures [16,29–32].

Table 1
Comparison of transient temperature θ at time $\xi = 0.05$ for $\beta = 1.0$, $T_E = 0.0$, $\omega = 0.5$, and $N = 0.1$ and two sets of wall reflectivities

ε_W	ε_E	Investigators	Transient temperature $\frac{T}{T_W}$		
			$x/X = 0.25$	$x/X = 0.50$	$x/X = 0.75$
1.0	1.0	Barker and Sutton [29]	0.4893	0.1775	0.0588
		Sutton [30]	0.4888	0.1778	0.0591
		Tsai and Lin [31]	0.4889	0.1773	0.0588
		Talukdar and Mishra [32]	0.4892	0.1768	0.0585
		Mishra and Lankadasu [16]	0.4893	0.1770	0.0584
		FVM–FVM (present)	0.4895	0.1771	0.0584
		LBM–FVM (present)	0.4897	0.1771	0.0581
1.0	0.0	Barker and Sutton [29]	0.5035	0.2003	0.0831
		Sutton [30]	0.5030	0.2005	0.0833
		Tsai and Lin [31]	0.5031	0.2001	0.0830
		Talukdar and Mishra [32]	0.5033	0.1995	0.0824
		Mishra and Lankadasu [16]	0.5029	0.2007	0.0829
		FVM–FVM (present)	0.4995	0.1995	0.0824
		LBM–FVM (present)	0.4996	0.1991	0.0820

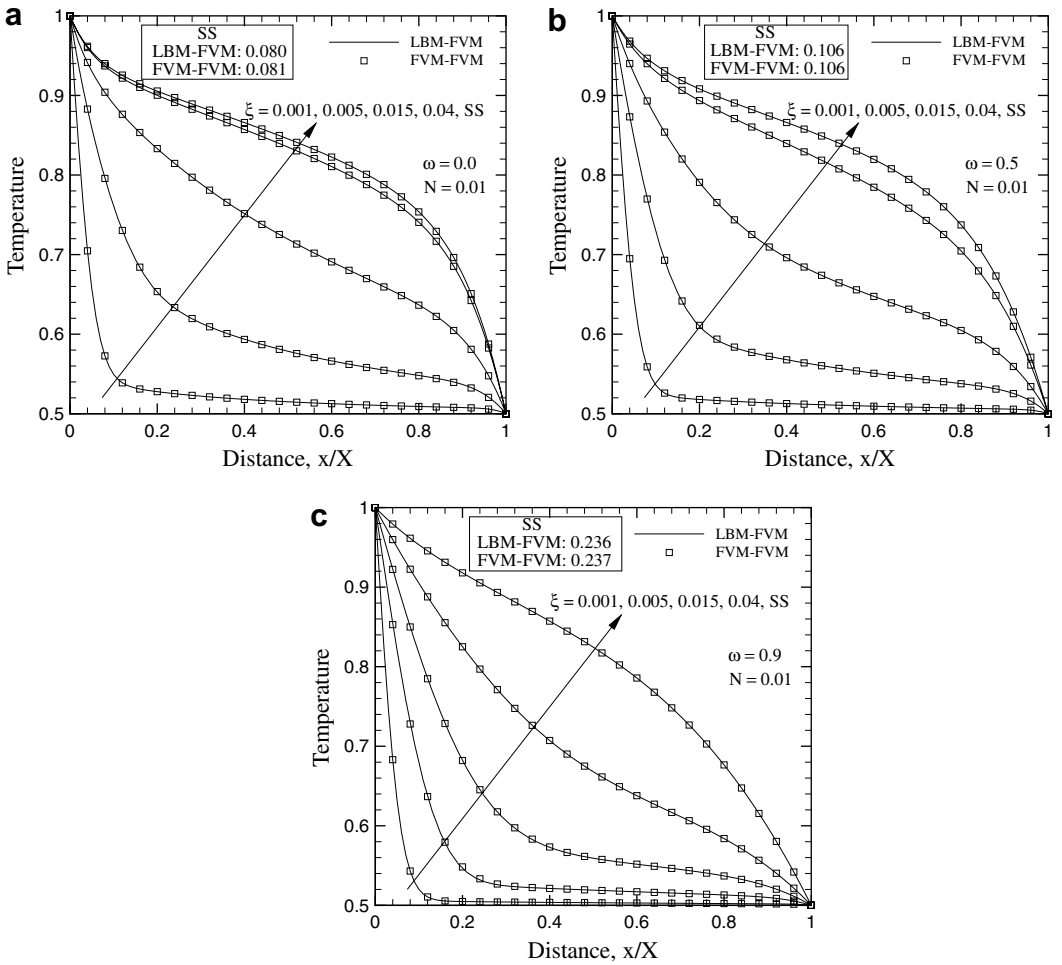

Fig. 5. Comparison of non-dimensional temperature T/T_W in a planar medium at different instants ξ for (a) scattering albedo $\omega = 0.0$ (a), 0.5 (b) and 0.9 (c).

Comparisons of the LBM–FVM and the FVM–FVM temperature T/T_W results at different instants of time ξ for various sets of parameters have been shown in Figs. 5–7. For results in these figures, the initial temperature of the system was T_E and for time $t > 0$, the west boundary was raised to a temperature $T_W = 2T_E$.

In Fig. 5a–c, for extinction coefficient $\beta = 1.0$ and conduction–radiation parameter $N = 0.01$, temperature T/T_W results of the FVM–FVM and the LBM–FVM have been compared at different instants of time ξ for three values of the scattering albedo $\omega = 0.0$, 0.5 and 0.9, respectively. It can be observed that at any ξ, the results of the two methods compare very well with each other and the LBM–FVM and the FVM–FVM are found to reach the steady-state (SS) almost the same time.

In Fig. 6, T/T_W results of the two methods have been compared for the effects of the conduction–radiation parameter N. For $\beta = 1.0$ and $\omega = 0.0$, in Fig. 6a–c, these comparisons have been shown for $N = 0.01$, 0.1 and 1.0, respectively. It is seen that for both radiation dominated ($N = 0.01$) (Fig. 6a) and conduction dominated ($N = 1.0$) (Fig. 6c) situations, results of the FVM–FVM and the LBM–FVM are in good agreements with each other. For $N = 0.1$ and 1.0, at an early stage $\xi = 0.001$, at some distance from the hot (west) boundary, the FVM–FVM results are ahead of the LBM–FVM results. This trend has also been observed before [16,18] while solving energy equations of the conduction–radiation problems using the LBM and the FVM in which radiative information $\nabla \cdot \vec{q}_R$ was computed either using the DTM or the CDM. Since the convergence rates are method specific, transient results may differ in some cases.

In Fig. 7, T/T_W results have been compared for the effects of the west boundary emissivity ε_W. For $\beta = 1.0$, $\omega = 0.0$ and $N = 0.01$, in Fig. 7a–c, comparisons have been shown for $\varepsilon_W = 0.1$, 0.5 and 0.9, respectively. In all

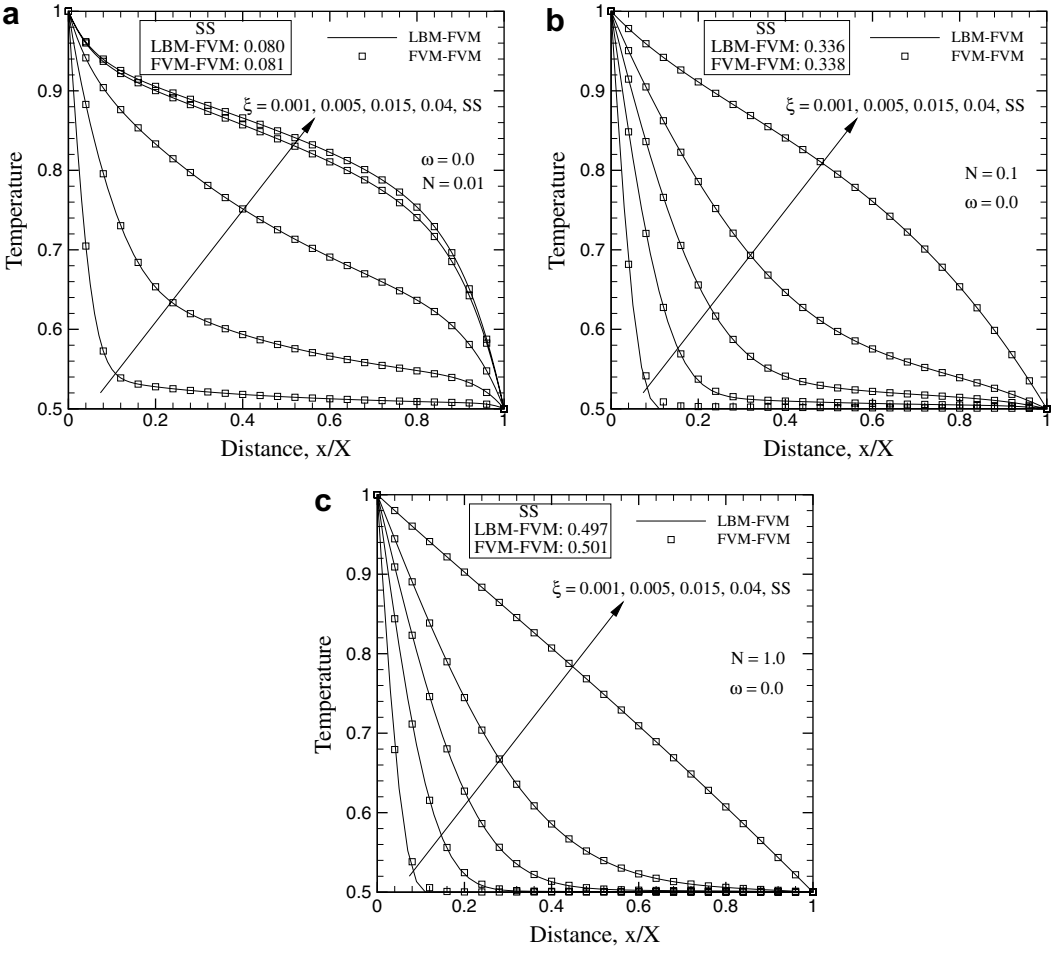

Fig. 6. Comparison of non-dimensional temperature T/T_W in a planar medium at different instants ξ for (a) conduction–radiation parameter $N = 0.01$ (a), 0.1 (b) and 1.0 (c).

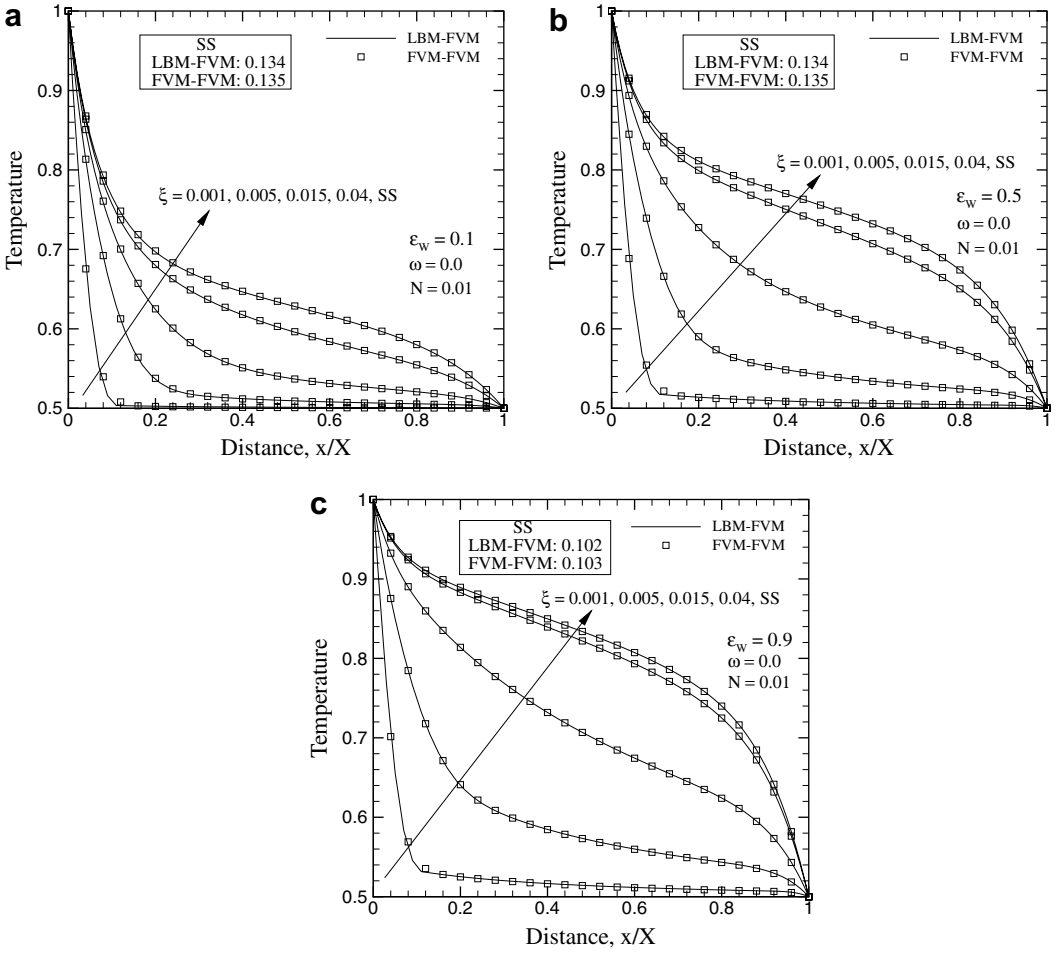

Fig. 7. Comparison of non-dimensional temperature T/T_W in a planar medium at different instants ξ for emissivity of the south boundary $\varepsilon_W = 0.1$ (a), 0.5 (b) and 0.9 (c).

these figures, the east boundary was considered black $\varepsilon_E = 1.0$. It can be seen from these figures that in all the cases, results of the FVM–FVM and the LBM–FVM match very closely with each other and the both the methods reach steady-state almost the same time.

Table 2
Effect of grid size in the FVM–FVM and the LBM–LBM on steady-state at three locations along the centerline $x/X = 0.5$

Control volumes/lattices	Number of directions $M_\theta \times M_\phi$	$y/Y = 0.3$		$y/Y = 0.50$		$y/Y = 0.7$	
		FVM–FVM	LBM–FVM	FVM–FVM	LBM–FVM	FVM–FVM	LBM–FVM
Effect of control volumes/lattices							
10×10	4×8	0.7608	0.7614	0.6649	0.6642	0.5973	0.5956
20×20	4×8	0.7591	0.7593	0.6641	0.6638	0.5965	0.5962
30×30	4×8	0.7591	0.7592	0.6638	0.6638	0.5964	0.5963
40×40	4×8	0.7590	0.7590	0.6638	0.6638	0.5964	0.5963
Effect of number of directions $M_\theta \times M_\phi$							
20×20	2×4	0.7710	0.7715	0.6608	0.6609	0.5794	0.5793
20×20	4×8	0.7591	0.7593	0.6641	0.6638	0.5965	0.5962
20×20	6×12	0.7598	0.7598	0.6637	0.6635	0.5969	0.5963

$\beta = 1.0$, $\omega = 0.0$, $N = 0.1$.

Table 3
Comparison of steady-state centerline ($x/X = 0.5$) temperature at three locations in a black square enclosure; $\omega = 0.0$, $\beta = 1.0$

N	Centerline T/T_S at y/Y	Wu and Ou [33]	Yuen and Takara [34]	Mishra et al. [35]	FDM–FVM	LBM–FVM
1.0	0.3	0.733	0.737	0.737	0.737	0.737
	0.5	0.630	0.630	0.630	0.630	0.630
	0.7	0.560	0.560	0.564	0.564	0.564
0.1	0.3	0.760	0.763	0.759	0.759	0.759
	0.5	0.663	0.661	0.663	0.664	0.663
	0.7	0.590	0.589	0.594	0.596	0.596
0.01	0.3	0.791	0.807	0.789	0.782	0.783
	0.5	0.725	0.726	0.725	0.726	0.725
	0.7	0.663	0.653	0.666	0.676	0.677

4.2. Combined conduction and radiation heat transfer in a 2-D square enclosure

Transient conduction and radiation heat transfer in a 2-D square enclosure (Fig. 2a) is considered next. In this, initially the entire system is at temperature $T_i = T_N = T_W = T_E$. For $t > 0$ the south boundary tempera-

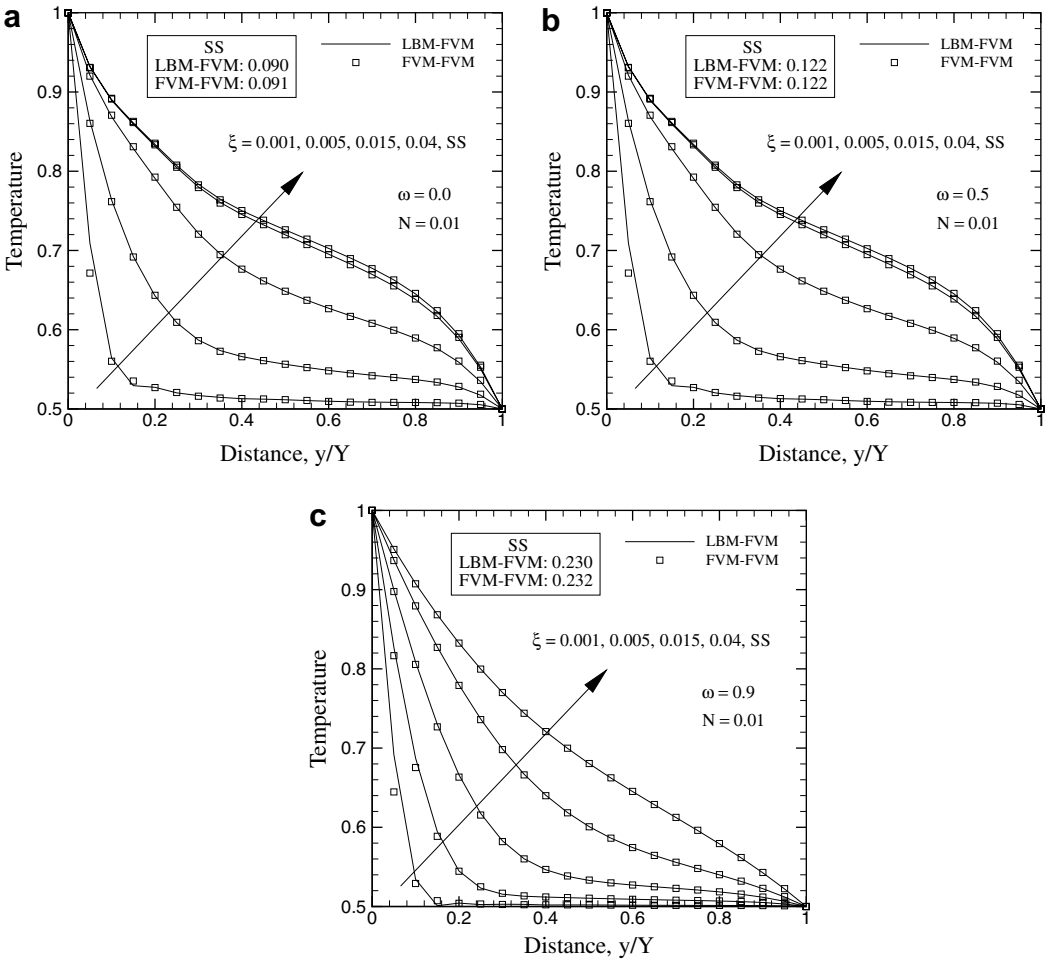

Fig. 8. Comparison of non-dimensional centerline temperature T/T_S in a 2-D square enclosure at different instants ξ for scattering albedo $\omega = 0.0$ (a), 0.5 (b) and 0.9 (c).

ture is raised to $T_S = 2T_i$. The enclosed gray-homogeneous medium is absorbing, emitting and isotropically scattering.

In Table 2, effects of the number of control volumes/lattices and the number of directions on temperature T/T_S results at three locations, *viz* $y/Y = 0.25$, 0.5 and 0.75 along the centerline $x/X = 0.5$ have been shown for the FVM–FVM and the LBM–FVM. These effects have been shown for the extinction coefficient $\beta = 1.0$, the scattering albedo $\omega = 0.0$ and the conduction–radiation parameter $N = 0.1$. Effect of the number of control volumes/lattices was studied for $M_\theta \times M_\phi = 4 \times 8$ directions and for the effect of the number of directions, 20×20 control volumes/lattices were considered in both the methods.

It can be seen from Table 2 that with $M_\theta \times M_\phi = 4 \times 8$, on 20×20 grids and larger, in both the FVM–FVM and the LBM–FVM, no significant variation in T/T_S is observed. A similar trend was also found for the other sets of parameters.

With 20×20 control volumes/lattices, effect of the number of discrete directions $M_\theta \times M_\phi$ on T/T_S results at three locations along the centerline $x/X = 0.5$ has also been shown in Table 2. No significant difference in the results are observed in $M_\theta \times M_\phi = 4 \times 8$ and $M_\theta \times M_\phi = 6 \times 12$. Hence for results in the following pages, in both the methods, we used 20×20 control volumes/lattices and $M_\theta \times M_\phi = 4 \times 8$ directions.

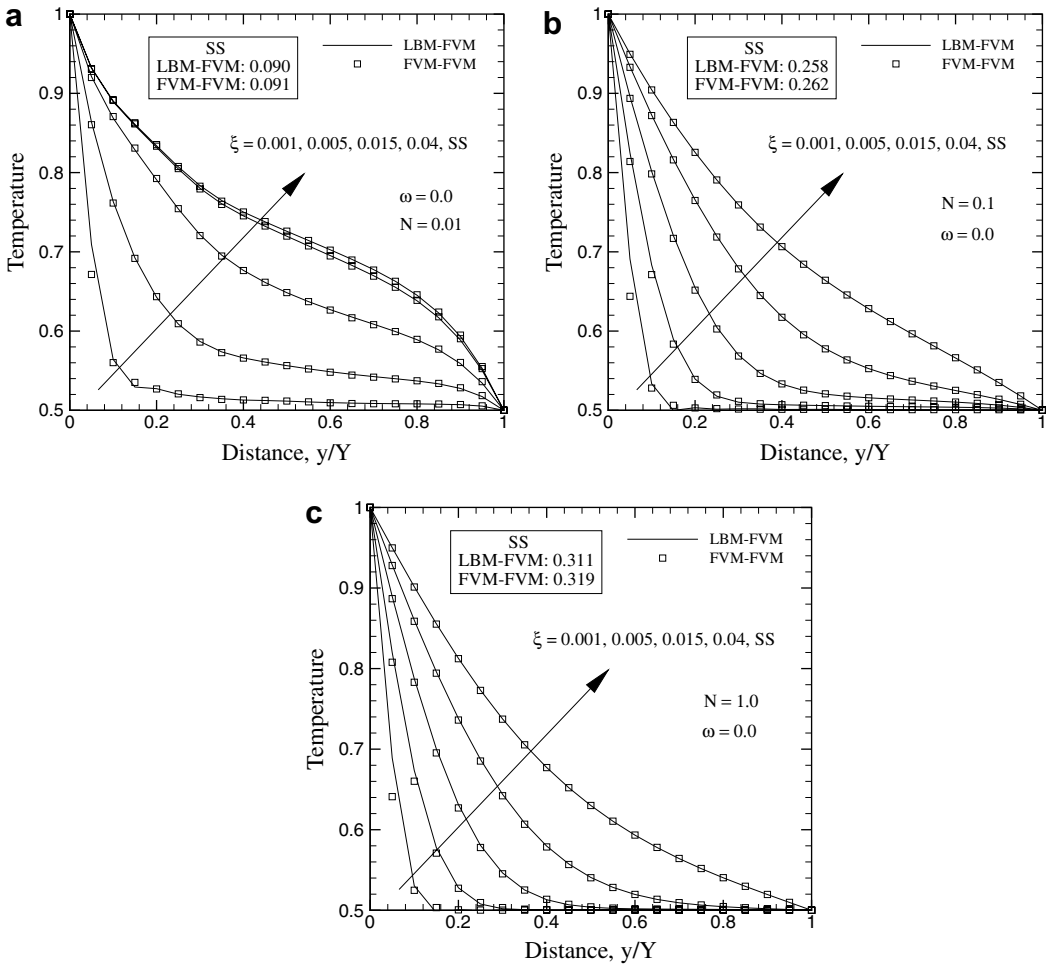

Fig. 9. Comparison of non-dimensional centerline temperature T/T_S in a 2-D square enclosure at different instants ξ for conduction–radiation parameter $N = 0.01$ (a), 0.1 (b) and 1.0 (c).

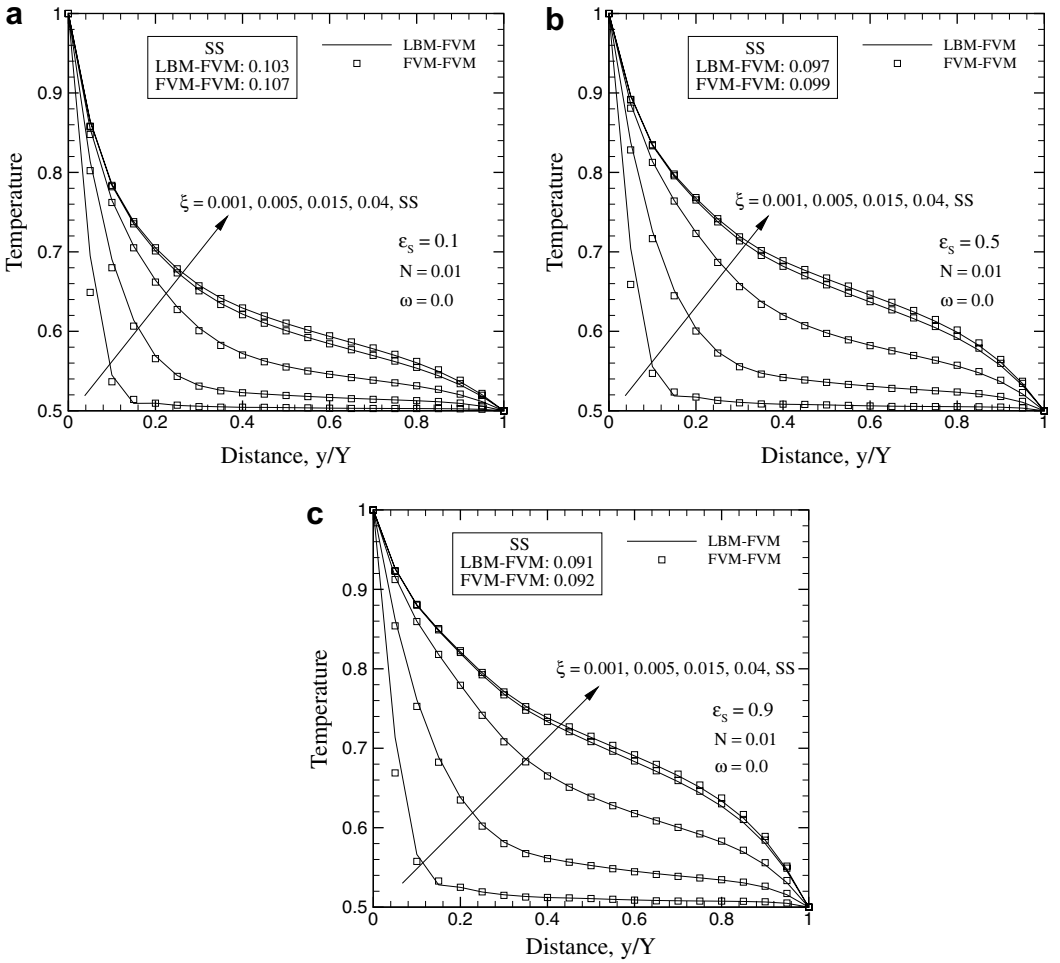

Fig. 10. Comparison of non-dimensional centerline temperature T/T_S in a 2-D square enclosure at different instants ξ for emissivity of the south boundary $\varepsilon_S = 0.1$ (a), 0.5 (b) and 0.9 (c).

In Table 3, for the absorbing emitting case $\omega = 0.0$ and extinction coefficient $\beta = 1.0$, for the three values of the conduction–radiation parameter N, temperature T/T_S results at three locations along the centerline ($x/X = 0.5$) are compared with those reported in the literature [33–35]. It is seen that the FVM–FVM and the LBM–FVM results compare very well with each other and with those reported in the literature [33–35].

Comparisons of the FVM–FVM and the LBM–FVM T/T_S results along the centerline ($x/X = 0.5$) for the effects of the scattering albedo ω, the conduction–radiation parameter N and the emissivity of the south boundary ε_S have been shown in Figs. 8–10, respectively. These results are shown for $\beta = 1.0$. In Figs. 8 and 9, all the four boundaries are considered black while for the results in Fig. 10, the south boundary is reflecting and other three boundaries are considered black.

It is seen from Figs. 8–10 that at all instants ξ, results of the FVM–FVM and the LBM–FVM are in very good agreements and the steady-state results match exactly with each other. Further it is observed that in all cases the LBM–FVM reaches steady-state slightly ahead of the FVM–FVM.

To have an idea of the number of iterations for the converged solutions and the CPU time required for the same, tests were performed with 20×20 and also with 40×40 control volumes/lattices. The LBM–FVM was found to take slightly less number of iterations and it was also computationally found slightly (1.03 times) faster than the FVM–FVM.

5. Conclusions

The LBM was used to solve the energy equations of transient conduction–radiation heat transfer problems in 1-D planar and 2-D square geometries containing an absorbing, emitting and isotropically scattering medium. Medium boundaries were considered diffuse-gray. To compare the performance of the LBM, energy equations of the problems were also solved using the FVM of the CFD. In the solution of the energy equations using the LBM and the FVM, the radiative information was computed using the FVM of the radiative heat transfer. For the same size of the control volumes and the lattices, in all the cases, results in both the FVM–FVM and the LBM–FVM were found in good agreements with those available in the literature and for various sets of parameters, they compared very well with each other. The number of iterations and the CPU times in the FVM–FVM and the LBM–FVM were found almost the same. The LBM–FVM was found slightly faster than the FVM–FVM.

The objective of the present work was to establish the compatibility of the FVM of the radiative heat transfer and the LBM for the solution of the energy equation of a combined conduction and radiation heat transfer. The FVM of the radiative heat transfer has emerged as one of the most versatile methods and the LBM is emerging as a potential complement of the CFD based methods. In the present work, with two simple geometries, with regard to the computational time, the LBM–FVM combination did not show any marginal advantage over the FVM–FVM. However, like fluid dynamics, even without parallelization, in complicated geometries and medium conditions, the LBM–FVM may have a gain over the FVM–FVM. Therefore, in combined radiation, conduction and/or convection heat transfer problems, use of the LBM for the solution of the energy equations and FVM for the calculation of radiative information should be further explored.

References

[1] F.J. Higuera, S. Succi, R. Benzi, Lattice gas dynamics with enhanced collisions, Europhys. Lett. 9 (1989) 345–349.
[2] F.J. Higuera, J. Jiménez, Boltzmann approach to lattice gas simulations, Europhys. Lett. 9 (1989) 663–668.
[3] R. Benzi, S. Succi, M. Vergassola, The lattice Boltzmann equation: theory and applications Authors, Phys. Rep. 222 (1992) 145–197.
[4] F. Massaioli, R. Benzi, S. Succi, Exponential tails in two-dimensional Rayleigh–Bénard convection, Europhys. Lett. 21 (1993) 305–310.
[5] S. Chen, G.D. Doolen, Lattice Boltzamann method for fluid flows, Ann. Rev. Fluid Mech. 30 (1998) 329–364.
[6] X. He, S. Chen, G.D. Doolen, A novel thermal model for the lattice Boltzmann method in incompressible limit, J. Comput. Phys. 146 (1998) 282–300.
[7] D.A. Wolf-Gladrow, Lattice-Gas Cellular Automata and Lattice Boltzmann Models: An Introduction, Springer-Verlag, Berlin-Heidelberg, 2000.
[8] S. Succi, The Lattice Boltzmann Method for Fluid Dynamics and Beyond, Oxford University Press, 2001.
[9] R.R. Nourgaliev, T.N. Dinh, T.G. Theofanous, D. Joseph, The lattice Boltzmann equation method: theoretical interpretation, numerics and implications, Int. J. Multipase Flow 29 (2003) 117–169.
[10] X. Shan, Simulation of Rayleigh–Benard convection using a lattice Boltzmann method, Phys. Rev. E 55 (1977) 2780–2788.
[11] A. Mezrhab, M. Bouzidi, P. Lallemand, Hybrid lattice-Boltzmann finite-difference simulation of convective flows, Comput. Fluids 33 (4) (2005) 623–641.
[12] J.R. Ho, C.-P. Kuo, W.-S. Jiaung, C.–J. Twu, Lattice Boltzmann scheme for hyperbolic heat conduction equation, Numer. Heat Transfer B 41 (2002) 591–607.
[13] J.R. Ho, C.-P. Kuo, W.S. Jiaung, Study of heat transfer in multilayered structure within the framework of dual-phase-lag heat conduction model using lattice Boltzmann method, Int. J. Heat Mass Transfer 46 (2003) 55–69.
[14] W.-S. Jiaung, J.R. Ho, C.-P. Kuo, Lattice Boltzmann method for heat conduction problem with phase change, Numer. Heat Transfer B 39 (2001) 167–187.
[15] D. Chatterjee, S. Chakraborty, An enthalpy-based lattice Boltzmann model for diffusion dominated solid–liquid phase transformation, Phys. Lett. A 341 (2005) 320–330.
[16] S.C. Mishra, A. Lankadasu, Analysis of transient conduction and radiation heat transfer using the lattice Boltzmann method and the discrete transfer method, Numer. Heat Transfer A 47 (2005) 935–954.
[17] N.G. Shah, A New Method of Computation of Radiation Heat Transfer in Combustion Chambers, Ph.D. thesis, Imperial College, University of London, England, 1979.
[18] S.C. Mishra, A. Lankadasu, K. Beronov, Application of the lattice Boltzmann method for solving the energy equation of a 2-D transient conduction–radiation problem, Int. J. Heat Mass Transfer 48 (2005) 3648–3659.
[19] S.C. Mishra, M. Prasad, Radiative heat transfer in absorbing-emitting-scattering gray media inside 1-D Cartesian enclosure using the collapsed dimension method, Int. J. Heat Mass Transfer 45 (2002) 697–700.

[20] R. Raj, Amit Prasad, P.R. Parida, S.C. Mishra, Analysis of solidification of a semitransparent planar layer using the lattice Boltzmann method and the discrete transfer method, Numer. Heat Transfer A 49 (2006) 279–299.
[21] N. Gupta, G.R. Chaitanya, S.C. Mishra, Lattice Boltzmann method applied to variable thermal conductivity conduction and radiation problems, J. Thermophys Heat Transfer, (2006), in press, doi:10.2514/1.20557.
[22] W.A. Fiveland, Three-dimensional radiative heat-transfer solutions by the discrete-ordinates method, J. Thermophys. Heat Transfer 2 (1988) 309–316.
[23] G.D. Raithby, E.H. Chui, A finite-volume method for predicting a radiant heat transfer in enclosures with participating media, J. Heat Transfer 112 (1990) 415–423.
[24] J.C. Chai, S.V. Patankar, Finite volume method for radiation heat transfer, Adv. Numer. Heat Transfer 2 (2000) 110–135.
[25] M.N. Borjini, C. Mbow, M. Daguenet, Numerical analysis of combined radiation and unsteady natural convection within a horizontal annular space, Int. J. Numer. Methods Heat Fluid Flow 9 (1999) 742–764.
[26] C.Y. Han, S.W. Baek, The effects of radiation on natural convection in a rectangular enclosure divided by two partitions, Numer. Heat Transfer A 37 (2000) 249–270.
[27] M.F. Modest, Radiative Heat Transfer, second ed., Academic Press, New York, 2003.
[28] T. Kush, B.S.R. Krishna, S.C. Mishra, Comparisons of the lattice boltzmann method and the finite difference methods for heat conduction problems, in: S.C. Mishra, B.V.S.S.S. Prasad, S.V. Garimella (Eds.), Proceedings of 18th National & 7th ISHMT-ASME Heat and Mass Transfer Conference, Guwahati, India, Tata McGraw Hill, New Delhi, 2006.
[29] C. Barker, W.H. Sutton, The transient radiation and conduction heat transfer in a gray participating medium with semi-transparent boundariesRadiation Heat Transfer, HTD-49, ASME, 1985, pp. 25–36.
[30] W.H. Sutton, A short time solution for coupled conduction and radiation in a participating slab geometry, J. Heat Transfer 108 (1986) 465–466.
[31] J.H. Tsai, J.D. Lin, Transient combined conduction and radiation with anisotropic scattering, J. Thermophys. Heat Transfer 4 (1990) 92–97.
[32] P. Talukdar, S.C. Mishra, Analysis of conduction and radiation heat transfer with heat generation in participating medium using the collapsed dimension method, Numer. Heat Transfer A 39 (2001) 79–100.
[33] C.Y. Wu, N.R. Ou, Transient two-dimensional radiative and conductive heat transfer in a scattering medium, Int. J. Heat Mass Transfer 37 (1994) 2675–2686.
[34] W.W. Yuen, E.E. Takara, Analysis of combined conductive–radiative heat transfer in a two-dimensional rectangular enclosure with a gray medium, J. Heat Transfer 110 (1988) 468–474.
[35] S.C. Mishra, P. Talukdar, D. Trimis, F. Durst, Computational efficiency improvements of the radiative transfer problems with or without conduction – a comparison of the collapsed dimension method and the discrete transfer method, Int. J. Heat Mass Transfer 46 (2003) 3083–3095.